EVS24
Stavanger, Norway, May 13-16, 2009

Investigation of Open-Circuit-Voltage Behaviour of Lithium-Ion Batteries with Various Cathode Materials under Special Consideration of Voltage Equalisation Phenomena

Jochen Bernhard Gerschler, Dirk Uwe Sauer
Institute for Power Electronics and Electrical Drives (ISEA), RWTH Aachen University
Jaegerstrasse 17-19, D-52066 Aachen, Germany
Phone: +49-241-8096970, Email: ge@isea.rwth-aachen.de

Abstract

Lithium-ion batteries show a complex behaviour regarding their open-circuit voltage (OCV). The OCV is influenced by previous operating condition and cannot be taken as independent from the operating history. A precise knowledge of the OCV is essential for many applications and battery models, since currently battery management systems use the well-defined OCV-SOC characteristic for state-of-charge estimation and power prediction. Especially lithium-ion batteries with iron-phosphate cathode material show a complex OCV behaviour including a hysteresis, which depends on the previous operation. In this paper several commercially offered lithium technologies are investigated and compared: Lithium-ion batteries with cathodes based on $LiNi_xCo_yAl_zO_2$ (NCA), $LiNi_xMn_yCo_zO_2$ (NMC) and iron-phosphate. The OCV characteristic of every system is analysed in-depth qualitatively and quantitatively. A special focus is on the factors influencing the occurring OCV, namely temperature, state-of-charge and previous history. OCV and hysteresis effects are investigated e.g. in self-discharge tests in order to analyse the long-term stability of hysteresis.

Lithium battery, battery management, open circuit, HEV, EV

1 Introduction

Lithium-ion batteries will be a part of next generation hybrid and full electric vehicles since power and energy density is superior to all other battery technologies. The introduction of lithium-ion batteries in series-production hybrid electric vehicles is announced by Daimler in the S400 Blue Hybrid for the 2nd half of this year, full electric vehicles with lithium-ion battery packs are already on the market based on battery packs with battery cells made for portable applications (e.g. Tesla, BMW Mini) and vehicles with special automotive proofed lithium-ion batteries are scheduled for 2010/2011. For sufficient power density and energy density lithium-ion systems employing cathode materials with mixed oxides such as $LiNi_xCo_yAl_zO_2$ (NCA) or $LiNi_xMn_yCo_zO_2$ (NMC) are used. Because of safety and cost issues olivine-type cathode materials, especially $LiFePO_4$, are getting more and more important. In the last

years the electrical properties are improved significantly by improvements in production methods and new materials.
But there are still some characteristics of $LiFePO_4$, which completely differ from competing cathode materials, namely $LiMO_x$- and manganese-spinel based cathodes. So the open-circuit voltage appears quite flat over a wide state-of-charge (SOC) range, furthermore the nominal voltage is less than the voltage of established materials, resulting in a lower energy density. Moreover $LiFePO_4$ shows a significant deviation between open circuit voltage (OCV) measured after previous charge and measured after previous discharge. The equilibrium potential is not unambiguously determined by the battery's state of charge (SOC) This deviation cannot be explained with time constants of typical diffusion processes only. Its impact factors seem to depend on the battery's operation history. Similar phenomena are also noticed for other lithium-ion batteries employing mixed-oxide cathodes. However, as these materials show a more severe dependency of the OCV on the SOC, the effects are of minor importance for the battery diagnostics. The phenomenon of OCV hysteresis is reported for NiMH batteries as well [3], [4].
An exact knowledge of OCV and its influencing factors is essential for many applications [1], [2]. In current battery management systems SOC estimation and power prediction are directly coupled to the well-defined OCV-SOC characteristics of most lithium-ion battery technologies. The accuracy of battery models is also directly affected by the accuracy of OCV calculation.
In this paper a comprehensive investigation of open-circuit voltage and voltage equalisation phenomena and their influencing factors is given for commercial lithium-ion systems. Considering the currently most promising Li-ion technologies this work presents results for systems with cathodes based on NCA, NMC and $FePO_4$. It is not in the scope of this paper, to give in-depth explanation for the basic electrochemical phenomena related to OCV hysteresis. A literature review shows indifferent explanation and modelling approaches, especially for iron phosphate. Rather this paper will give a quantitative and qualitative analysis in order to initiate and fructify the development of a physico-chemical and phenomenological open-circuit voltage model as a subject of further work.

2 Survey of equilibrium voltage and hysteresis phenomena

Physical and electrochemical behaviour of a Li-ion battery is defined by the chemical composition and the structure of its anode and cathode. While today's Li-ion batteries mostly use a carbon or rather graphite based anode, the diversity of cathode materials is high. While $LiCoO_2$ is first choice in consumer applications as laptops, the next generation HEV and EV will use mixed oxide cathodes (NCA, NMC) or $LiFePO_4$.
This section will give a survey of equilibrium voltage and hysteresis phenomena or rather effects which are related to these issues. The review bases upon results already published in literature.
One of the first who reported on hysteresis and memory effects in lithium batteries were Sleight et. al. [5]. They observed a voltage hysteresis effect depending on sign of the previous current. This was explained by a first-order phase transition when Li is inserted in Li_xMnO_2. Furthermore they determined an influence on previous history of cell operation called "new terrain" effect. The "new terrain" effect is traced back to the idea of Li_xMnO_2 as a disordered two-phase system, with memory of the previous cycles stored through the positions of phase boundaries. In two phase systems hysteresis is caused by dissipation energies when phase transitions take place in the crystal structure of the electrode. A voltage hysteresis is also reported by Barker et. al. [6] for a Li_xCoO_2 system. As the Li-metal system, Li_xCoO_2 shows two-phase transition during intercalation and deintercalation of Li-ions in the cathode structure. The hysteresis effect for Li_xCoO_2 is noticed as relatively small and explained by thermodynamically properties during phase transition processes. The structural changes in $LiCoO_2$ systems and their two-phase transition characteristics are also discussed by Carlier et. al. [7]. According to them a two-phase transition is represented by voltage plateaus in the OCV-SOC characteristics of a system. This is in agreement with a constant value of lithium chemical potential measured in the mean time.
In recent years a lot of work is done on the field of phosphor-olivine structured cathode materials, mainly lithium iron phosphate ($LiFePO_4$). One of the first who reported on the structure and behaviour of phosphor-olivine structured electrodes were Padhi et. al. [9]. They give an explanation for the insertion process of Li-ions in a $FePO_4$ structure. Furthermore they noticed the flat open-circuit characteristic of $LiFePO_4$ and reduced

these results to structural changes during chemical delithiation of $LiFePO_4$ or rather lithiation of $FePO_4$. The changes can be summarised as a first-order transition in the phosphor-olivine crystal structure.
The phase structure is further investigated by Dodd et. al. [10]. They studied the transformation of the two-phase mixture, $xLiFePO_4$ and $(1\text{-}x)FePO_4$, to a single-phase Li_xFePO_4 for several compositions x and found some hysteresis caused by this phase transition process.
The charge/discharge characteristics of $LiFePO_4$ electrodes is investigated in-depth by Srinivasan and Newman. They developed a discharge model for these electrodes, the so called shrinking-core approach [11], which displays the juxtaposition of the two phases mentioned above in an iron-phosphate system and the movement of the phase boundary. The shrinking-core approach with its hard phase boundaries, and thus pre-history influenced potential boundaries, seem to be a suitable approach for explanation of equilibrium voltage and hysteresis effects on electrode materials showing a two-phase transition. The same authors enhanced their model approach in [12] finding the existence of path-dependence or rather impact of previous (cycling) history on the behaviour of $LiFePO_4$.

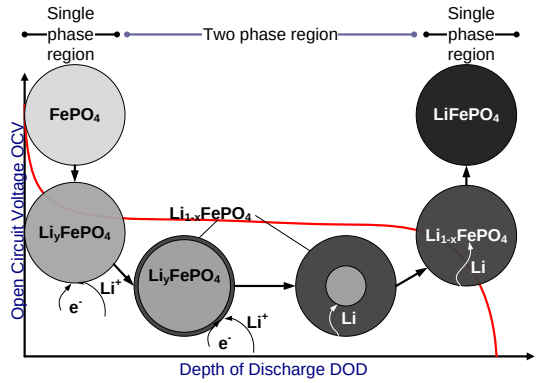

Figure 1: Phase transition in particles on the cathode of a $LiFePO_4$ system during discharge [12]

Zhang and White established a similar modelling approach for the $LiCoO_2$ electrode [8]. Thus the shrinking-core model approach seems to be a suitable approach for description for all electrodes showing a first-order phase transition.
Zheng et. al [14], [15] noticed hysteresis effects related to lithium insertion in carbons, i. e. anode materials for lithium-ion batteries. During their studies they found a clear relationship between hydrogen content of the carbon materials and the characteristic of the occurring voltage hysteresis. The hysteresis effect is explained by interaction between Li-ion and hydrogen-containing carbon structure during intercalation: When inserting lithium in the carbon, some lithium atoms bind on the hydrogen-terminated edges of carbon fragments. In order to intercalate, lithium must overcome an energy barrier before it can bonded near hydrogen. The energy barrier seems to control the size of the hysteresis. Thus, lower hydrogen content means a lower energy barrier and less hysteresis.
Similar to effects reported on $LiCoO_2$ and $LiFePO_4$ cathodes, which are shown earlier in this section, Yazami et. al. [17] also described phase or rather structure transition on graphite anodes. Depending on the degree of lithiation or rather delithiation, the graphite shows a plateau in its voltage characteristics – a hint for a two phase system showing LiC_{12} and LiC_6 stages. The transition process between the two stages is characterised by a hysteresis, which could be caused by entropy changes during intercalation processes.
Summarising the review there is not yet a clear and substantive explanation of hysteresis phenomena in lithium-ion batteries. There are many indications that hysteresis effects are caused by phase-transition processes, but a final proof for this hypothesis is still lacking. Moreover an interaction between effects occurring on the anode and the cathode of the Li-ion systems cannot be excluded.

3 Experimental

In context of this work different Li-ion battery technologies are investigated. The systems employed in the measurements are specified in Table 1. The following subsections describe the applied test procedures.

3.1 OCV characteristics

OCV characteristics are measured on fully charged cells by discharging with 0.5 C-rate in 5 % or rather 10 % ΔDOD steps until end-of-discharge voltage (EODV) is reached. The pause after the discharge steps has a duration of 3 h. In charge direction the measurement is repeated reversely by charging the cells with 0.5 C-rate until end-of-charge voltage (EOCV) is reached. In order to investigate temperature dependency of OCV the measurements are carried out at T = -10°C, 23°C, and 50°C.

Table 1: Lithium-ion batteries employed in this work

Label	Cathode material	Anode material	Electrode design	Nominal voltage	Nominal capacity	Application
Type A	$Ni_{0.33}Mn_{0.33}Co_{0.33}O_2$ (NMC)	Hard carbon	Pouch, high power	3.5 V	6.0 Ah	HEV
Type B	$Ni_xCo_yAl_zO_2$ (NCA)	Carbon	cylindrical, high power	3.6 V	7.2 Ah	HEV
Type C	$FePO_4$	Carbon	cylindrical, high power	3.3 V	2.3 Ah	Power tools

3.2 Relaxation of overvoltages

This set of measurements is performed to verify that a hysteresis is really present even after long rest periods. Vanishing effects after long rest periods are only diffusion processes. Furthermore the effect of temperature is analysed. Measurements are carried out at three different operating points (DOD = 25 %, 50 %, 75 %), which are adjusted by employing a current rate of 0.5 C-rate. After adjustment of DOD levels the cell voltage is logged for 24 h. The measurements are performed both after previous discharge and previous charge. For investigation of possible temperature impacts on relaxation and diffusion processes the tests are performed at five test temperatures
(T = -20°C, -10°C, 0°C, 23°C, 50°C).
For advanced analysis the charge/discharge current-rate for adjustment of DOD levels is varied in order to determine possible impacts of current rates on the relaxation of overvoltages and hysteresis.

3.3 Influence of the previous history on relaxation and hysteresis effect

In order to get a better understanding of relaxation and hysteresis processes are influenced by cell's previous history, the above explained test procedure is modified: the test only considers voltage equalisation at DOD = 50%, both after several previous discharging and charging scenarios. The cell voltage is logged during a 12 h rest period. The discharge or rather charge scenarios vary in charge throughput per time. The target SOC is adjusted using different numbers of equidistant DOD step widths having varying rest periods in between:

Scenario 1
After cells have been fully charged the target DOD = 50 % is adjusted by discharging with 0.5 C-rate in one step followed by a 12 h rest period. After that cell is completely discharged and target DOD is adjusted by 0.5 C-rate charging, also followed by a 12 h rest period.

Scenario 2
Now the cells are adjusted in two discharge or rather two charge steps with ΔDOD = 25 %. After each step a varying rest period of 1 h, 3 h or 6 h is performed. At DOD = 50 % the rest period has a duration of 12 h both after discharge and charge pre-history.

Scenario 3/ 4
Scenario 3 is similar to scenario 2 described above. Instead of two steps of ΔDOD = 25 %, this scenario is characterised by five equidistant discharge/ charge steps of ΔDOD = 10 % for adjustment of target DOD.
Scenario 4 schedules ten equidistant discharge or rather charge steps of ΔDOD = 5 %.

Scenario 5
In context of this procedure both the current impact on voltage equalisation and open circuit voltage is determined:
The current impact on voltage equalisation process and OCV is tested by modifying scenario 3. Instead of using 0.5 C-rate the discharge and charge steps employ current-rates of 2 C-rate or rather 5 C-rate.

3.4 Investigation of paths between OCV limiting curves – impact of Ah amount on hysteresis

Thele [4] reports on inner voltage curves between the charge and discharge OCV boundary curves for NiMH when operating with charge amounts not bigger than a battery specific value Q_{hyst_max}. After charging or discharging a charge amount $|Q| > Q_{hyst\_max}$ the OCV returns to the outer OCV curves which occur during pure discharging or charging. It is the goal of this set of tests to investigate, if such phenomena also exist for Li-ion batteries or rather such a specific charge amount as found for NiMH batteries can also be determined for lithium-ion systems. Finding such a relationship would be of importance for the interpretation of the OCV-DOD relation in micro or rather partial cycle dominated operation with charge amounts less than the above mentioned boundary value Q_{hyst_max}.

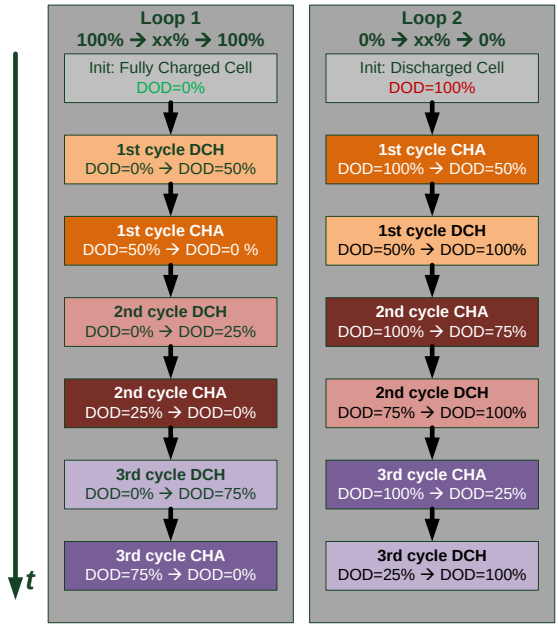

Figure 2: Sequences for investigating of paths between limiting OCV boundary curves when employing partial cycles. In "loop 1" (left-hand chart) partial cycles start on a fully charged cell, in "loop 2" (right-hand plot) cycles start on completely discharged cell

The test is carried out both starting on a fully charged and on a completely discharged cell:
In the first scenario (left-hand chart in Figure 2) the fully charged cell is discharged with 0.5 C-rate in steps of ΔDOD = 5 % until DOD = 50 % is reached having a 3 h rest period after each discharge step (1st cycle DCH). At the end of each pause the OCV is measured. Then the cell is charged employing 0.5 C-rate until reaching EOCV (1st cycle CHA). The same procedure is repeated as discharge/ charge to DOD = 25 % (2nd cycle) and DOD = 75 % (3rd cycle).
The second loop (right-hand chart in Figure 2) starts with completely discharged cells. In a 1st cycle cells are charged in 5 % ΔDOD steps to DOD = 50 %, then the cells are discharged with the same step width until EODV is reached. After a rest period of 3 h following each step the OCV is measured. Analogical to the first scenario the measurement is also repeated for target DOD of 75 % (2nd cycle) and 25 % (3rd cycle).
In an additional test scenario a partial cycle typical for HEV applications is investigated: The cell is discharged to DOD = 50 % followed by a charge with 0.5 C-rate in steps of 2.5 % ΔDOD until DOD = 30 % is reached. Each charge step is followed by a 3 h rest period for OCV determination. From DOD = 30 % the test is performed contrarily by discharging the system in steps of 2.5 % ΔDOD until the initial DOD of 50 % is reached again.

3.5 Temperature impact on OCV

In order to investigate the temperature impact on OCV cell types A, B and C are fully charged and adjusted to a DOD of 50 %. After a rest period of 12 h for decay of relaxation and faster diffusion processes, temperature inside a temperature chamber is changed from an initial value of T = 50 °C to T = -30 °C during a time period of 24 h. Afterwards cells' temperature is changed vice versa by raising the temperature from T = -30 °C to T = 50 °C in the same time period as for cooling down.

3.6 Impact of self discharge on OCV hysteresis

In order to investigate the long-term stability of hysteresis affected by self discharge a 14 weeks storage test is carried out. Target DOD of 50 % is adjusted by previous discharge of the fully charged cell or rather charge of the completely discharged cell employing 0.5 C-rate. After conditioning, the cells are put in an oven at T = 40 °C for accelerating self discharge processes. OCV is logged daily during the tests.

3.7 Test equipment

All tests are carried out at battery test benches made by DIGATRON firing circuits. The used circuits have a maximum charge/discharge current rate of 50 A or rather 100 A and a voltage/ current accuracy of ± 0.5 % related to the set-point. During long-term equilibrium measurements and self discharge tests cell voltages are logged with a FLUKE 289 multimeter having an accuracy of ± 1 mV.

4 Results

4.1 Relaxation of overvoltages – equilibrium voltage

Lithium-ion batteries show hysteresis phenomena, which cannot be explained by diffusion and relaxation processes only. In this chapter voltage equalisation and its influencing factors are investigated more in-depth. In the further context "hysteresis" of OCV describes a thermodynamically steady difference between OCV after previous charge and OCV after previous discharge. At this point all relaxation or rather diffusion processes caused by states of disequilibrium inside the battery have decayed. It is often difficult to differentiate between a real hysteresis effect and a virtual hysteresis. A virtual hysteresis describes a difference between OCV still occurring after a rest period of a few hours, when slow and very slow solid-state diffusion processes are still ongoing.

4.1.1 Impact of temperature and SOC

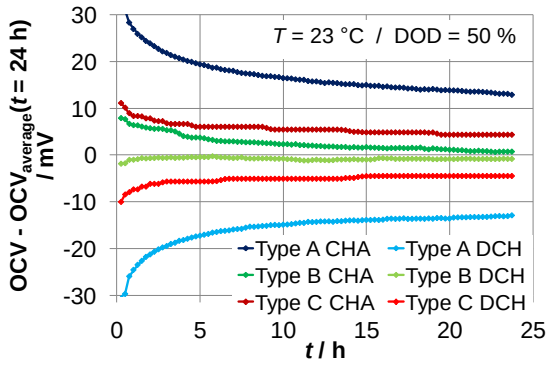

Figure 3: Voltage equalisation vs. time during a 24 h rest period at T = 23 °C and DOD = 50 % for cell types A, B and C. The current OCV is subtracted from the average of OCV(t = 24 h) after charge and discharge for each cell type.

To get a general understanding about voltage equalisation of cell types A, B and C, the OCV deviation of all three types is plotted over time during a 24 h rest period both after charge and discharge. For better comparison of the different cell types the OCV is subtracted from the average OCV after charge and discharge at t = 24 h for each system. The measurement is carried out at T = 23 °C, the cells are charged or rather discharged to a target DOD of 50 %.

Figure 3 shows the voltage relaxation of the three cell types. From the plot it can be derived that NCA material (type B) shows least ΔOCV after 24 h, NMC material (type A) shows the highest ΔOCV. Depending on the cell type the first few hours after DOD adjustment are dominated by relaxation and faster diffusion processes, over a longer time span slower solid-state diffusion processes become predominantly. Effects of self-discharge, which are typical in the range of 3 % - 5 % DOD per month (0.1 % - 0.16 % DOD per day) at room temperature, might be negligible against these processes within a time span of 24 h. Comparison of the three systems show a fast decay of overvoltages for type B. Formation of OCV after discharge takes place nearly completely within the first two hours. Type B shows an asymmetric decay of overvoltages depending on the previous step. OCV after discharge is faster in steady state than OCV after previous charge; in the end its ΔOCV is negligible with less than 2 mV considering the error of measurement. Cell type A shows a significantly slower relaxation process than type B. Moreover curves both after charge and discharge show still a slope in OCV at t = 24 h. The fact that both OCV curves are still sloping could indicate that equalisation processes, which might be mainly solid-state diffusion processes, are still taking place. Especially after t = 3 h curves show a significant relaxation, this issue has to be considered in the measurement of OCV characteristics presented in 4.2.1. In contrast type C is virtually in steady state after 3 h, difference between OCV at t = 3 h and t = 24 h is less than 1.5 mV. Further changes in the voltages might be caused by slow solid state diffusion processes.

To further investigate influencing factors on voltage equalisation ΔOCV of type A and C is plotted over time at several temperatures. For better data analysis ΔOCV is normalized to its values at t = 24 h for each cell type at each

temperature. From Figure 4 it can be derived that temperature influences voltage equalisation significantly, especially within the first few hours after DOD adjustment. This is the time span in which faster relaxation and diffusion processes in the electrolyte and inside the intercalation electrodes are predominantly, which are highly sensitive on temperature.

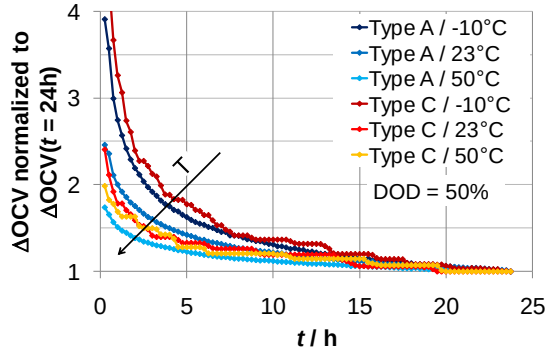

Figure 4: ΔOCV vs. time for cell type A und C at DOD = 50 % for several test temperatures

The plot shows the fastest voltage equalisation at the highest test temperature (T = 50 °C) for both cell types, a clear characteristic for the relaxation and diffusion processes within this time span. The impact of temperature on voltage equalisation appears quite comparable for types A and C.
In Figure 5 ΔOCV of type A and C is plotted over time at T = 23 °C for several depths of discharge. As in Figure 4 ΔOCV is normalized to the 24 h value of each type at each DOD.
It is obvious that DOD influences the voltage relaxation. At lower DOD the decay of ΔOCV appears much faster than at medium and higher DOD. This effect might be caused by the behaviour of either cathode or anode, one of the electrodes seem to limit the equalisation process

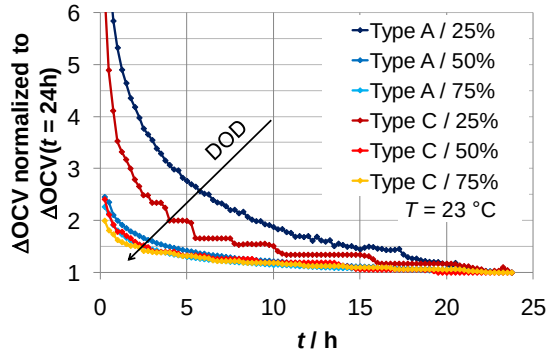

Figure 5: ΔOCV vs. time for cell type A and C at T = 23 °C and several DOD

for low DOD, this issue should be further investigated by half-cell measurements, which were not performed in context of this work.

4.1.2 Impact of pre-history and current-rate

As already reported by [11], [12] and [13] the equilibrium voltage of iron-phosphate based systems is influenced by the previous operation history of the systems. Within this paper investigations are performed where DOD is adjusted by varying the capacity throughput or rather the current-rate per time as described in 3.3, a more detailed investigation for iron-phosphate can be found in the work of Roscher[13].

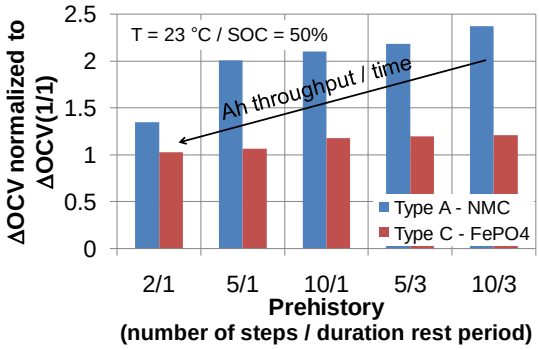

Figure 6: ΔOCV influenced by pre-history for cell type A (blue-coloured bars) and type C (red-coloured bars). DOD = 50 % is adjusted in different ways (different step sizes (% DOD) and varying duration of rest periods (hours) between the steps) employing 0.5 C-rate charge/ discharge current. ΔOCV values are related to one-step adjustment of target DOD.

Figure 6 shows the impact of different ways of DOD adjustment on the OCV hysteresis for cell types A and C. A target DOD of 50 % is adjusted by using a varying number of steps with equidistant ΔDOD and a varying rest period between the charge/ discharge steps (according to test procedure described in 3.3). ΔOCV is normalized to the one step scenario employing a direct adjustment with a current of 0.5 C-rate to DOD = 50 % both by charge and discharge. From the plot it can be observed qualitatively for both type A and type C, that an increasing capacity throughput within a time span lowers the occurring hysteresis voltage. The same result can be found in a second test scenario which varies the current rate in addition to number of steps and rest period. ΔOCV is also normalized to values at one step adjustment employing 0.5 C-rate. Employing 5 C-rate instead of 0.5 C-rate seems to halve hysteresis for both systems, a hint for an

apparent current dependency of ΔOCV. The same scenario is repeated with five steps of 10 % ΔDOD for adjustment of target DOD with a rest period of 3 h in between, both employing 0.5 C-rate and 5 C-rate. The higher C-rate also lowers ΔOCV in the 5/3 scenarios, but the current impact now appears much weaker than in the 1/1 scenarios. (ΔOCV is only approx. 6 % (type A) or rather 9 % (type C) smaller for using 5 C-rate in the 5/3 scenario compared to 5/3 adjustment employing 0.5 C-rate)
Knowing that a higher capacity throughput per time or rather a higher current-rate causes a higher internal cell temperature, the apparent current impact on hysteresis could partly or completely be a temperature impact.

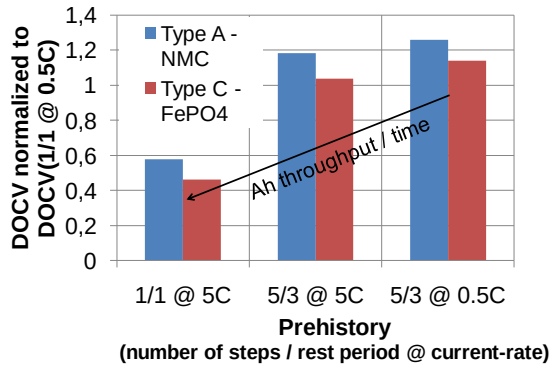

Figure 7: Normalized ΔOCV after different pre-histories varying number of steps, duration of rest period and current-rate. Results are plotted for cell type A (blue bars) and type C (red bars), ΔOCV is related to scenario (1/1) employing a current of 0.5 C-rate

4.1.3 Long-term relaxation processes

Results in 4.1.1 show that a rest period of 24 h is not enough time for the system to reach steady state conditions. In an additional test types A, B and C are charged or rather discharged to a target DOD of 50 % employing 0.5 C-rate, the cell voltage and the hysteresis ΔOCV is plotted during a 100 h rest period, temperature is held constantly at T = 23 °C.
Figure 8 shows the behaviour of type A over time. After 100 h difference between OCV after previous charge and discharge is approx. 1 mV, since this is a value inside the error of measurement the hysteresis virtually decays during the rest period. While the OCV curve after charge shows an average gradient of approx. -1 mV/ 20 h between 20 h and 100 h, the OCV after discharge rises until t = 70 h, before the values begin to decrease. The long-term measurement of type A might show a superposition of slow solid-state diffusion processes and self-discharge. For time spans longer than 70 h self discharge becomes predominantly. Both processes lead to a virtual disappearance of hysteresis for cells with NMC material.

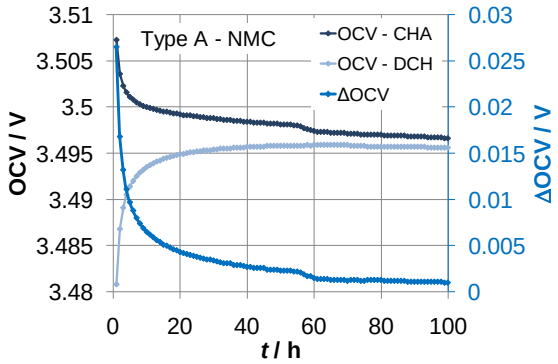

Figure 8: Voltage equalisation of type A during a 100 h rest period after previous charge or rather discharge with 0.5 C-rate. (DOD = 50 %, T = 23 °C)

In contrast type C seems to show a hysteresis as defined above based on results plotted in Figure 9 where the same test as for type A is performed for iron-phosphate material. After 100 h ΔOCV is approx. 4.7 mV. In section 4.5 the test for iron-phosphate material is extended to 14 weeks at T = 40 °C to further investigate the impact of self discharge on hysteresis.

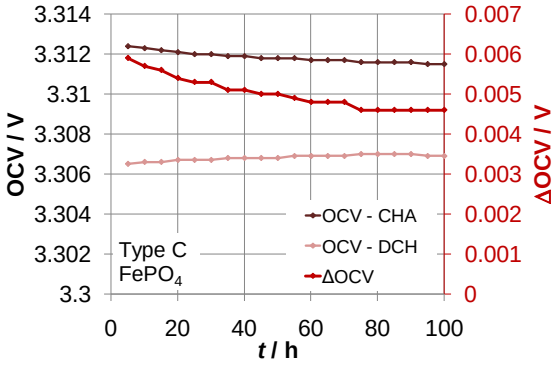

Figure 9: Voltage equalisation of cell type C after previous charging/ discharging. (DOD = 50 %, T = 23 °C)

4.2 OCV characteristics

4.2.1 NMC – Type A

The OCV characteristics of cell type A are measured according to the test procedure described above in section 3.1. In Figure 10 the OCV characteristics after previous discharge are plotted over DOD at T = -10 °C, 23 °C and 50 °C test temperature.

In a first approximation the curves show a quite linear behaviour over DOD with a gradient of approx. -15 mV / % DOD at T = 23 °C, plateaus in the OCV characteristics as reported for iron-phosphate or $LiCoO_2$ cannot be noticed. A temperature dependency can also be found. With increasing temperature the level of the OCV decreases slightly, this effect appears most distinctively for medium and higher DOD. Moreover the OCV gradient shows a slight rise with increasing temperature (approx. -13 mV / % DOD at T = -10 °C and -15.5 mV / % DOD at T = 50 °C). In parts a higher OCV with decreasing temperatures might be caused by slower relaxation of overvoltages according to 4.1.1. In order to quantify the virtual hysteresis effect the difference between OCV after previous charging and discharging is plotted over DOD in Figure 11 for the same test temperatures and rest period as plotted in Figure 10. The plot shows parabola-shaped curves for all three test temperatures with a maximum occurring between 60 % and 75 % DOD. For T = -10 °C the maximum difference is 57 mV, at T = 23 °C 60 mV and at T = 50 °C 80 mV. These results are quite noteworthy, especially their dependency on

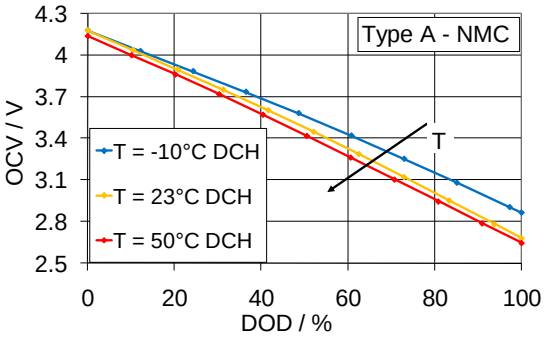

Figure 10: OCV characteristics of cell type A measured at T = -10 °C, 23 °C and 50 °C after previous discharge (DCH) (3 h rest at each DOD level)

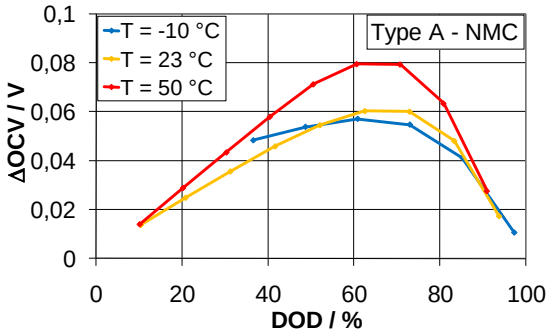

Figure 11: Difference ΔOCV of cell type A between OCV curves after charge and discharge plotted over DOD at T = -10 °C, 23 °C and 50 °C

temperature. Within minutes to hours after adjusting a certain DOD level diffusion and relaxation should be dominating processes. Since diffusion and relaxation processes run faster at higher temperatures (see section 4.1), highest test temperature should show the smallest ΔOCV. Considering the results presented in the previous section, results presented in Figure 11 are not fully understood yet.

4.2.2 NCA – Type B

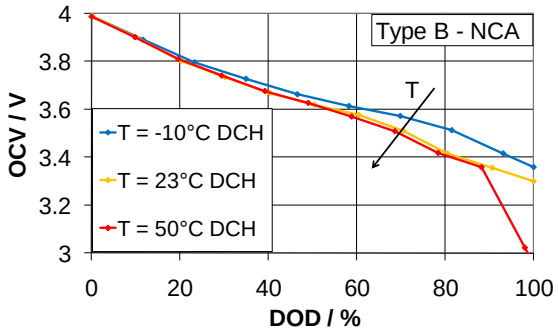

Figure 12: OCV after previous discharge as a function of DOD for cell type B with NCA material measured at different temperatures

As already observed for type A with NMC material, OCV characteristic of type B with NCA material (Figure 12) shows a steady slope, the gradient at T = 23 °C is approx. -7 mV/ % DOD. The temperature impact on OCV appears similar to type A, the tendency of decreasing OCV level with increasing temperature can also be observed for NCA material. This might be caused by faster relaxation of overvoltages within the 3 h pause at elevated temperatures.

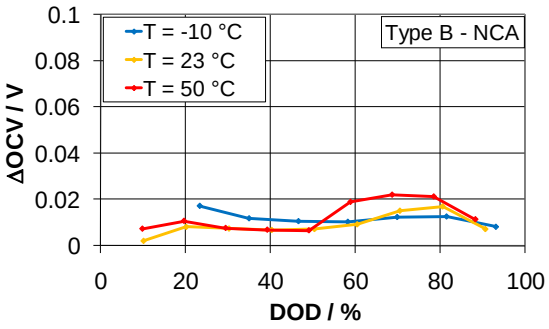

Figure 13: Hysteresis ΔOCV between OCV curves after charging and discharging of type B plotted over DOD for several test temperatures

As already observed in 4.1 compared to type A the hysteresis between OCV after charge and discharge is less than type A (Figure 13). A clear temperature impact on hysteresis cannot be found, but tendency that ΔOCV appears higher with higher temperatures and maxima occurring at higher DOD can be also observed. It is noteworthy that ΔOCV shows its maxima between 60 % and 80 % DOD; within this gap the OCV characteristics show a slight plateau. Considering the gradient of the OCV characteristics over DOD and the occurring ΔOCV, hysteresis of type B is virtually negligible for technical purposes.

4.2.3 Type C –$FePO_4$

In contrast to metal-oxide based cathode materials iron-phosphate shows a quite different OCV characteristic. In Figure 14 it can be observed that the OCV vs. DOD characteristic of type C shows a gradient between 10 % and 70 % DOD of only 46 mV or -0.8 mV/ % DOD (charge OCV curve, T = 23 °C) which is one order of magnitude less compared with results obtained for type A and type B. Moreover plateaus in the upper OCV curve between DOD = 10 %...25 % and DOD = 60 %...70 % can be noticed. The lower OCV curve (after previous discharge) seems to be a bit depressed compared to the OCV curve after previous discharge. The 1st plateau appears slightly shorter (DOD = 10 %...20 %), a 2nd plateau occurs between 40 %...60 % DOD. The gradient of the lower OCV curve is bigger than the gradient of the upper curve, especially the decrease between 60 % and 80 % DOD appears stronger. This result in a significant hysteresis of OCV as already reported in section 4.2.1 for type A. ΔOCV is plotted over DOD in Figure 15. Compared to type A with NMC material the ΔOCV of $FePO_4$ appears more asymmetrical showing nearly a "M"-shaped curve with local maxima occurring between 25 % and 40 % DOD and between 65 % and 75 % DOD and a local minimum between 50 % and 60 % DOD. Maxima in hysteresis occur close to plateaus of the OCV characteristic. The asymmetry of OCV characteristics is a hint, that processes, which lead to plateaus in the OCV vs. DOD characteristic might start at different DOD depending on previous history. The asymmetric character of OCV of type C also affects paths between the boundary OCV occurring for partial cycles, this issue is further investigated in 4.4.

A comparison of ΔOCV curves at different temperatures show an indifferent temperature impact on hysteresis for type C. While the first maximum shows higher ΔOCV with decreasing temperature, the second maximum is nearly unaffected by cell temperature.

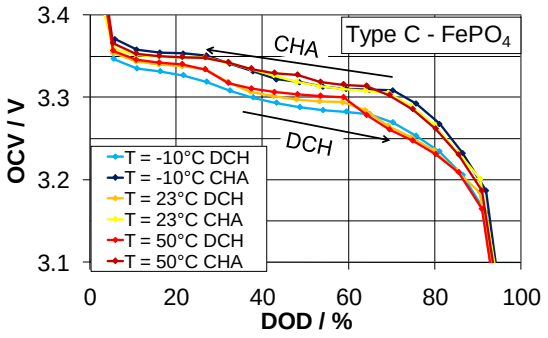

Figure 14: OCV characteristics of type C plotted over DOD for several test temperatures after previous charge or rather discharge

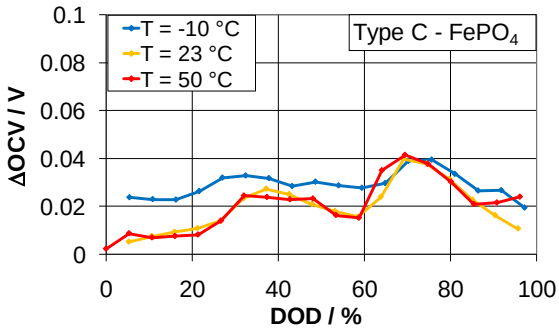

Figure 15: OCV hysteresis of cell type C plotted vs. DOD for different temperatures

In contrast to NCA- and NMC-based cells the OCV characteristics of type C show only a very slight temperature dependency. The level of OCV appears slightly rising with increasing

temperatures, but a clear temperature – OCV relation cannot be determined.

4.3 Temperature impact on equilibrium voltage and OCV

As already reported in the sections above, OCV shows a slight temperature impact. In order to investigate this issue more in-depth and to give an estimation for self-discharge impacts, cells' voltage is logged over temperature when cooling down from T = 50 °C to T = -30 °C during a time period of 24 h, afterwards cells' temperature is changed vice versa as described in 3.5.
In Figure 16 OCV variation is plotted over temperature, temperature variation is related to OCV at T = 50 °C. It can be noticed that type A shows a negative temperature coefficient, while NCA and $FePO_4$ show a positive temperature coefficient. The OCV of all systems varies by an amount of approx. 10 mV over a temperature range between -30 °C and 50 °C. The OCV vs. T behaviour is superposed by slow diffusion processes and self discharge resulting in a hysteresis, which is characterized by an expansion of the curves for higher temperatures (approx. 2 mV – 3 mV).

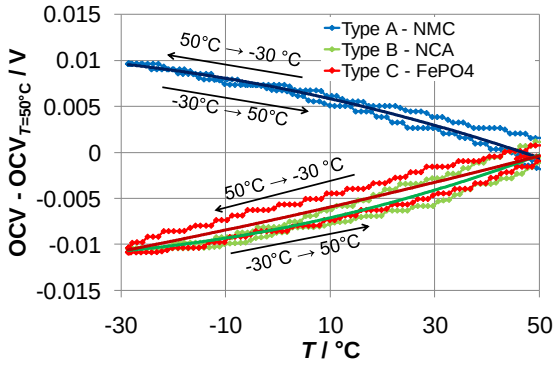

Figure 16: Temperature impact on cell voltage: ΔOCV vs. time for cell type A, B and C, voltage difference is related to OCV at T = 50 °C, steps in the curves are caused by limited resolution in the temperature measurement

4.4 Path between limiting OCV curves

Figure 17 shows paths between limiting OCV boundary curves (grey dotted lines) when performing the test sequence "loop 1" according to 3.4 and Figure 2. From the plot it can be derived that cell type C shows a completely different behaviour than reported for NiMH by [4]. From the performed discharge/charge cycles no specific charge amount can be identified which shifts the OCV voltage back to one or the other boundary curve. The results for the three cycles appear indifferent: While in the 3rd cycle (ΔDOD = 75 %) the charge OCV boundary curve is already reached after a charge amount of 5 % ΔDOD (and falls under the boundary curve again when leaving the plateau in charge direction), the 1st and 2nd cycle show a completely different behaviour: The OCV paths run between the boundary OCV curves and reach the upper boundary curve in the plateau of the charge OCV curve between 10 %...15 % DOD, resulting in a charge amount for reaching the upper curve of approx. 30 % ΔDOD for the 1st cycle and approx. 10 %...15 % ΔDOD for the 3rd cycle.

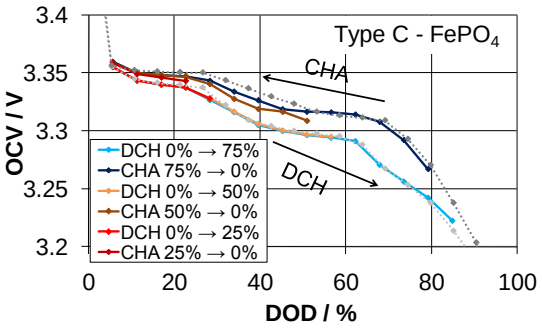

Figure 17: Paths between limiting OCV curves for partial discharges with DOD = 25 %, 50 % and 75 % and following full charge. Test is carried out employing cell type C at T = 23 °C, test starts with fully charged cell (DOD = 0 %)

The second test scenario "loop 2" described in section 3.4 starting with a completely discharged cell shows also an indifferent behaviour regarding charge amount necessary for changing the boundary OCV curve: While the 75 % ΔDOD charge/ discharge cycle reaches the lower OCV boundary curve already after a ΔDOD of 5 % and undershoots the boundary curve slightly in the following, the 25 % and 50 % charge/ discharge cycles reach the boundary curve almost for DOD > 90 %. It is noteworthy that the discharge paths do not run to an equal end value for DOD < 90 %. For type C a charge amount dependency does not seem to exist for running to the boundary curves. Moreover the paths seem to be affected by their cycle depth since differences in plateaus and gradients can be noticed. Considering the results from Figure 17 and Figure 18 it seems that the reproducibility of the paths in fitting the plateaus and slopes in between of boundary OCV is quite critical, a possible hint

that formation of plateaus in OCV may be influenced by pre-history of operation.

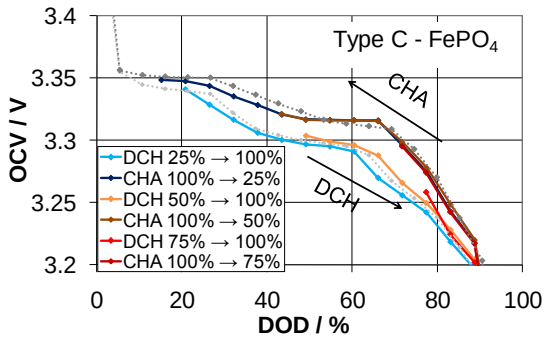

Figure 18: Paths between limiting OCV curves in an inversely scenario as plotted in Figure 17 starting with a completely discharged cell (DOD = 100 %)

The problem of OCV paths between the boundary OCV curves can be determined as quite significant by a third test scenario described in 3.4: Starting on the discharge OCV boundary curve at DOD = 50 % the cell is charged in steps of 2.5 % ΔDOD. The OCV measured after the charge steps follows a path which appears nearly in parallel to upper boundary curve (distance between upper boundary curve and path reduces only 4 mV with 10 % ΔDOD).

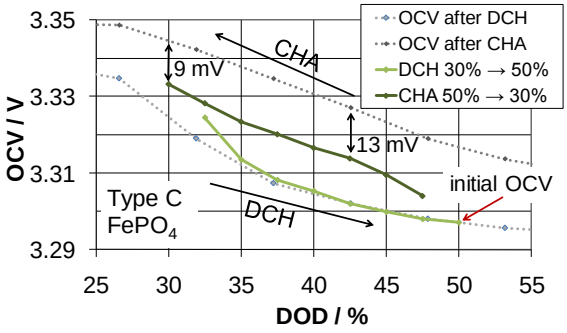

Figure 19: OCV vs. time for type C during charge from DOD = 50 % to 30 % starting on the OCV discharge curve. Charge is followed by discharge back to initial DOD.

Tests are also performed with cell type A. Independent from cycle depth of partial cycles their OCV paths do not reach the boundary curves, neither in loop 1 nor in loop 2. Moreover "sub"-hysteresis loops can be detected.

4.5 Impact of self discharge on OCV

While hysteresis vanishes for type A and B virtually within a time span of 100 h, hysteresis of type C appears to be more long-term stable. To further investigate this issue, cell type C is charged or rather discharged to DOD = 50 % and stored for 14 weeks at T = 40 °C. During the test period, the OCV is logged on the charged and discharged cell. OCV and ΔOCV are plotted over time in Figure 20. It can be observed that both OCV after charge and after discharge decrease over time caused by self-discharge. Since the gradient of OCV after charge appears slightly bigger than gradient of OCV after discharge the hysteresis also decreases under the impact of self discharge. After 14 weeks hysteresis is less than 2 mV, a value which is virtually negligible considering the error of measurements. As for type A, self discharge lead to a vanishing hysteresis of OCV, though within a significant longer time span.

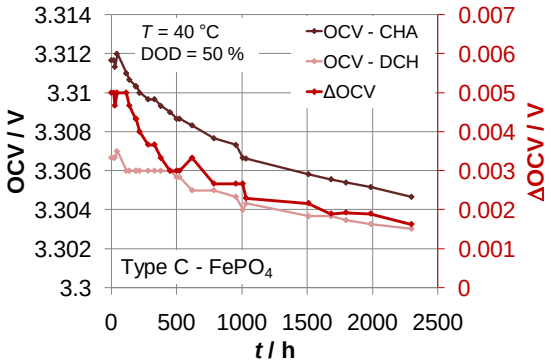

Figure 20: OCV after previous charge or rather previous discharge vs. time during a 14 weeks storage test at T = 40 °C. The red curve shows development of voltage hysteresis ΔOCV during the test period

5 Discussion

The measurements have identified the OCV as something which is well deviating from equilibrium voltage in a thermodynamic definition. The measured OCV is a complex superposition of relaxation, diffusion and self-discharge processes on the one hand and a hysteresis caused by different material phases on the other hand. It seems to be hardly possible to isolate the single processes which occur, when current is cut-off. During the first period of time the OCV is dominated by faster relaxation and diffusion processes and shows a clear dependency on cell temperature and DOD. Afterwards, the OCV is dominated by slower solid-state diffusion processes and self-discharge. A comparison of cell types A, B and C shows that hysteresis of OCV seems to be a question of definition and

considered time period. Hysteresis phenomena nearly vanish for all systems, but even in different time periods. For type B decay of ΔOCV is dominated by faster relaxation and diffusion processes, the decay of ΔOCV of type A is characterised by a superposition of very slow solid-state diffusion processes and self-discharge. Type A is an example for a system showing a so called virtual hysteresis, because its ΔOCV is of relevance for technical issues since typical time constants in HEV and EV are in the range of a few minutes up to hours, where ΔOCV is not negligible. A similar tendency of ΔOCV decay can be observed for type C, though within a significant longer time span (time span of a few days for type A against time span of a few month for type C). Self discharge results in a de facto disappearance of hysteresis within a time period of 2-3 months. From a technical point of view OCV hysteresis is a quite critical issue considering the flat OCV characteristics of iron phosphate cathode materials. In worst case a SOC/ DOD determination based on OCV can cause an error of more than 40 %. Especially in the typical operation range of battery systems for HEV, which is typical 40 %...70 % SOC, a SOC determination seems to be challenging. Type C shows most obviously the relation between plateaus in OCV vs. DOD characteristics, which are caused by phase transitions within the active material, and maxima in hysteresis. Moreover the indifferent impact of temperature of hysteresis over DOD, especially at the maxima, might be a hint for the existence of different material phases showing a differing temperature dependency. The impact of these different phases has to be further investigated since it influences the paths between the OCV boundary curves, which occur during technically most relevant micro and partial cycle operation. From the results it seems to be likely that hysteresis phenomena are mainly caused by the cathode and its characteristics.

Another issue which is not fully understood yet is the impact of previous history on virtual hysteresis or rather hysteresis. From the measurements carried out in context of this work an impact of capacity throughput or rather current rate per time could be determined: The higher the capacity throughput or rather the current rate per time, the lower the hysteresis. A higher current rate per time yields a higher local heating inside the active mass accelerating relaxation shortly after current is cut off. These temperature effects could superpose current impacts on hysteresis. Impact of previous history should also be an issue of further research. Foremost it is essential to design test procedures which ensure temperature equilibrium inside the cell to uncouple current from temperature impacts.

Considering the results it has to be noticed that investigations were performed with power cells with NMC, NCA and $FePO_4$ cathode material. The results found within this work are confirmed using energy cells of the same manufacturers having a comparable anode and cathode material. Nevertheless it is likely that relaxation and diffusion is strongly dependent on characteristics of the anode and cathode material including variations in the stoichiometry of the mixed oxides or the coating of the iron phosphate based cathode. Moreover the composition of cell and the manufacturing process might yield different OCV phenomena. So it seems to be necessary to extend the investigation of the hysteresis topic to other lithium-ion systems to get a more balanced overview. In spite of these uncertainties about behaviour of other NMC, NCA and $FePO_4$ systems this work gives a fundamental analysis of hysteresis phenomena in currently most promising lithium-ion systems.

References

[1] O. Bohlen, J. Gerschler, D. Sauer, P. Birke, M. Keller. *Robust Algorithms for a Reliable Battery Diagnosis - Managing Batteries in Hybrid Electric Vehicles* 22nd Electric Vehicle Symposium (EVS22), Yokohama, Japan, Oct. 2006

[2] M. Dubarry, V. Svoboda, R. Hwu, B. Y. Liaw. *Capacity loss in rechargeable lithium cells during cycle life testing: The importance of determining state-of-charge*; J. Power Sources 174 (2007) 1121 – 1125.

[3] M. Verbrugge, E. Tate. *Adaptive state of charge algorithm for nickel metal hydride batteries including hysteresis phenomena*; J. Power Sources 126 (2004) 236 – 249.

[4] M. Thele, O. Bohlen, D. U. Sauer, E. Karden. *Development of a voltage-behaviour model for NiMH batteries using an impedance-based modeling concept*. J. Power Sources 175 (2008) 635 – 643

[5] A. K. Sleight, J. J. Murray, W. R. McKinnon. *Memory effects due to phase conversion and hysteresis in Li/LixMnO2 cells*; Electrochimica Acta Vol. 36, No. 9, 1469-1474, 1991

[6] J. Barker, R. Pynenburg, R. Koksbang, M. Y. Saidi. *An electrochemical investigation into the lithium insertion properties of LixCoO2*; Electrochimica Acta Vol. 41, No. 15, 2481-2488, 1996.

[7] D. Carlier, I. Saadoune, M. Ménétrier, C. Delmas. *Lithium Electrochemical Deintercalation from O2-LiCoO2 – Structure and Physical Properties*; J. Electrochem. Soc. 149 (10) A1310-A1320, 2002.

[8] Q. Zhang, R. E. White. *Moving Boundary Model for the Discharge of a LiCoO2 Electrode*; ECS Transactions, 6(22) 33-52, 2008.

[9] A. K. Padhi, K. S. Nanjundaswamy, J. B. Goodenough. *Phospho-olivines as Positive-Electrode Materials for Rechargeable Lithium Batteries*; J. Electrochem. Soc. 144 (4) 1188-1194, 1997.

[10] J. L. Dodd, R. Yazami, B. Fultz. *Phase Diagram of LixFePO4*; Solid-State Letters, 9(3) A151-A155, 2006.

[11] V. Srinivasan, J. Newman. *Discharge Model for the Lithium Iron-Phosphate Electrode*; J. Electrochem. Soc. 151(10) A1517-A1529, 2004.

[12] V. Srinivasan, J. Newman. *Existence of Path-Dependence in the LiFePO4 Electrode*; Solid-State Letters 9(3), A110-A114, 2006.

[13] M. A. Roscher, J. Vetter, D. U. Sauer. *Influence of cathodes technology on the power capability and charge acceptance of lithium-ion batteries*, poster presentation at EVS 24, 2009.

[14] T. Zheng, Y. Liu, E. W. Fuller, S. Tseng, U. von Sacken, J. R. Dahn. *Lithium Insertion in High Capacity Carbonaceous Materials*; J. Electrochem. Soc. 142(8), 2581-2590, 1995.

[15] T. Zheng, W. R. McKinnon, J. R. Dahn. *Hysteresis during Lithium Insertion in Hydrogen-Containing Carbons*; J. Electrochem. Soc. 143(7), 2137-2145, 1996.

[16] T. Zheng, J. R. Dahn. *Hysteresis observed in quasi open-circuit voltage measurements of lithium insertion in hydrogen-containing carbons*; J. Power Sources 68 (1997) 201-203.

[17] R. Yazami, Y. Reynier. *Thermodynamics and crystal structure anomalies in lithium-intercalated graphite*; J. Power Sources 153 (2006), 312-318.

Authors

Jochen Bernhard Gerschler received his diploma in electrical engineering from University of Dortmund. In July 2005 he joined Institute for Power Electronics and Electrical Drives of RWTH Aachen University as a research engineer. His research activitities include characterisation, diagnostics, and electrical, thermal and lifetime modelling of NiMH- and Li-ion batteries

Dirk Uwe Sauer, Prof. Dr. rer.nat., studied Physics at University of Darmstadt. From 1992-2003 he has been research scientist and senior scientist at Fraunhofer Institute for Solar Energy Systems ISE in Freiburg/Germany. In 2003, he received his PhD at Ulm University on battery modelling and system optimization. In 2003 he was a appointed as a Juniorprofessor at RWTH Aachen University for "Electrochemical Energy Conversion and Storage Systems". He published more than 200 papers and presentations in international journals, conferences and books